Signatures of non-Loudon-Fleury Raman scattering in the Kitaev magnet β-Li₂IrO₃

Yang Yang ¹, Yiping Wang, ² Ioannis Rousochatzakis ³, Alejandro Ruiz, ⁴ James G. Analytis, ^{5,6} Kenneth S. Burch ³, ² and Natalia B. Perkins ¹

¹School of Physics and Astronomy, University of Minnesota, Minneapolis, Minnesota 55455, USA
²Department of Physics, Boston College, Chestnut Hill, Massachusetts 02467, USA
³Department of Physics, Loughborough University, Loughborough LE11 3TU, United Kingdom
⁴Department of Physics, University of California, San Diego, California 92093, USA
⁵Department of Physics, University of California, Berkeley, California 94720, USA
⁶Materials Sciences Division, Lawrence Berkeley National Laboratory, Berkeley, California 94720, USA

(Received 11 February 2022; revised 30 April 2022; accepted 11 May 2022; published 2 June 2022)

We investigate the magnetic excitations of the hyperhoneycomb Kitaev magnet β -Li₂IrO₃ by means of inelastic Raman scattering. The spectra exhibit the coexistence of a broad scattering continuum and two sharp low-energy peaks at 2.5 and 3 meV, with a distinctive polarization dependence. While the continuum is suggestive of fractional quasiparticles emerging from a proximate quantum spin liquid phase, the sharp peaks provide the first experimental signature of the "non-Loudon-Fleury" one-magnon scattering processes proposed recently [Yang *et al.*, Phys. Rev. B **104**, 144412 (2021)]. The corresponding microscopic mechanism is similar to the one leading to the symmetric off-diagonal exchange interaction Γ (because it involves a combination of both direct and ligand-mediated exchange paths) but is otherwise completely unexpected within the traditional Loudon-Fleury theory of Raman scattering. The present experimental verification therefore calls for a drastic reevaluation of Raman scattering in similar systems with strong spin-orbit coupling and multiple exchange paths.

DOI: 10.1103/PhysRevB.105.L241101

Introduction. In recent years, magnetic insulators of 4d and 5d transition metal compounds with bond-directional exchange anisotropies, broadly known as Kitaev materials, have become a rich playground for novel magnetic phases of matter [1–9]. The majority of these systems order magnetically at sufficiently low temperatures [8,9], consistent with theoretical predictions that the Kitaev quantum spin liquid (QSL) phases, which are stabilized by the so-called Kitaev anisotropy K, are fragile against weak perturbations [3,10–12]. However, the usual dominance of the Kitaev coupling causes these materials to be in relative proximity to the ideal QSL phases, leading to a general expectation that the magnon modes expected at low energies will coexist with a broad continuum associated with the fractional excitations (spinons) of the nearby QSL phases [13–22].

Here we explore this picture in the hyperhoneycomb Kitaev material β -Li₂IrO₃ with inelastic Raman scattering, which is known to be a sensitive probe of single- and multiparticle excitations over sufficiently wide ranges of temperature and energy [15,18,19,21]. The β -Li₂IrO₃ compound features an Fddd orthorhombic space group, with a hyperhoneycomb lattice of Ir⁴⁺ ions, each forming an effective $J_{\rm eff} = 1/2$ magnetic moment due to strong spin-orbit coupling (SOC) [22–27]. As shown in Fig. 1(a), the Ir⁴⁺ ions form zigzag chains (red and green bonds) running alternatively along the ($\mathbf{a} - \mathbf{b}$, $\mathbf{a} - \mathbf{b}$) and ($\mathbf{a} + \mathbf{b}$, $\mathbf{a} + \mathbf{b}$) directions. At zero field and below $T_I = 38$ K, the system shows an incommensurate (IC) order with counterrotating spin sublattices and propagation wave vector $\mathbf{Q} = (0.574, 0, 0)$ in orthorhombic

units [23,24]. This complex order results from the competition among various bond-dependent anisotropic exchange interactions. Similar to all other Kitaev materials [8,9], edge-sharing IrO₆ octahedra in β -Li₂IrO₃ provide 90° paths for the dominant bond-directional, Ising-like Kitaev interaction among magnetic moments [2,3]. Besides the dominant Kitaev anisotropy, β -Li₂IrO₃ features additional interactions, such as the nearest-neighbor (NN) Heisenberg interaction J and the symmetric component of the NN off-diagonal exchange coupling, commonly referred to as the Γ interaction [11,28,29].

In agreement with earlier studies by Glamazda *et al.* [15], our experimental results for the Raman susceptibility reveal a broad scattering continuum that survives in a wide temperature range up to 100 K, well above T_I . Our analysis of the T dependence of this continuum and the evolution of its spectral weight, as well as a comparison with theoretical calculations, suggests that this continuum is not associated with the magnon excitations of the low-T ordered phase. Rather, the continuum is more consistent with spinons of the proximate Kitaev spin liquid phase, thus reinforcing the magnon-spinon dichotomy picture previously advocated for this material by a resonant inelastic x-ray scattering study [22].

In addition to the continuum background, however, we have observed two sharp, low-energy peaks below T_I , which were not resolved in Ref. [15]. These peaks appear in cross polarization and not in the parallel polarization and, furthermore, disappear above T_I . A direct comparison of these findings with the recently [30] revised theory of Raman scattering, applicable to Kitaev-like Mott insulators with strong SOC,

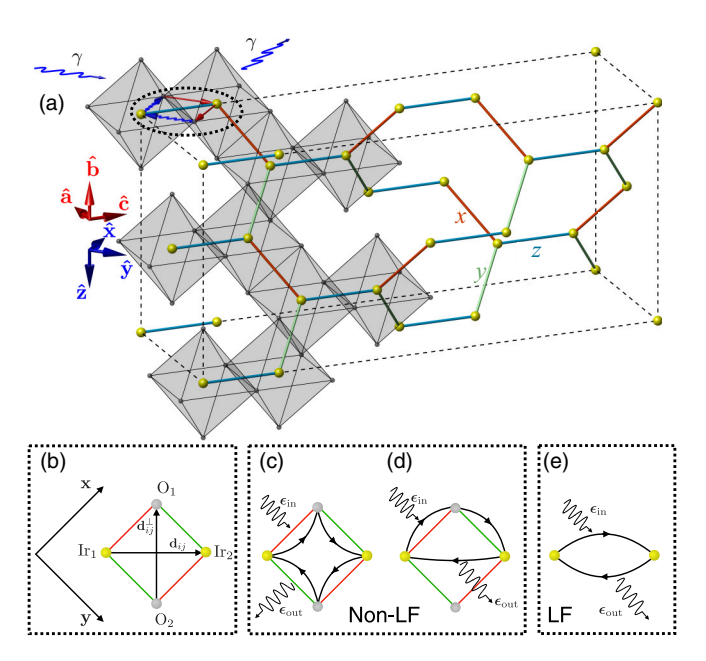


FIG. 1. (a) Hyperhoneycomb network of Ir^{4+} ions (yellow spheres) in β -Li₂IrO₃. Each octahedron denotes an IrO₆ cage. (b) All microscopic processes leading to the effective Hamiltonian on a given bond are confined to the Ir₂O₂ plaquette [also highlighted in (a) by a black dashed circle]. (c) and (d) Non-Loudon-Fleury Raman processes, in which the virtual, photon-assisted, electron hopping process does not reduce to the effective Hamiltonian multiplied by an overall polarization dependence factor, as in (e) typical LF processes.

reveals that these peaks are, in fact, an experimental signature of "non-Loudon-Fleury" magnon scattering processes. More specifically, according to Ref. [30], the leading contributions to the Raman vertex \mathcal{R} [which enters the Raman intensity $\mathcal{I}(\Omega) \propto \int dt \ e^{i\Omega t} \langle \mathcal{R}(t) \mathcal{R}(0) \rangle$, where $\Omega = \omega_{\text{in}} - \omega_{\text{out}}$ is the total energy transfer and $\langle \cdots \rangle$ denotes thermal averaging] contain significant terms arising from microscopic photonassisted tunneling processes [Figs. 1(c) and 1(d)] beyond those [Fig. 1(e)] appearing in the traditional Loudon-Fleury (LF) theory [31,32]. Among these, the virtual processes in Fig. 1(d), which involve both direct and ligand-mediated paths, are of type similar to the ones leading to the symmetric off-diagonal interaction Γ , but in the Raman vertex, they take the form of a bond-directional magnetic dipole term. Such terms are responsible for the appearance of sharp, one-magnon Raman peaks with distinctive polarization dependence and are otherwise not expected in the traditional LF theory [30].

Crystal growth, handling, and characterization. High-quality single crystals of β -Li₂IrO₃ were grown by a vapor transport technique. Ir (99.9% purity, BASF) and Li₂CO₃ (99.999% purity, Alfa-Aesar) powders were ground and pelletized at 3000 psi in a molar ratio of 1:1.05. The pellets were placed in an alumina crucible, reacted for 12 h at 1050 °C, and then cooled down to room temperature at 2 °C/h to yield single crystals which were then extracted from the reacted powder. β -Li₂IrO₃ crystallizes in the orthorhombic Fddd space group and averages $105 \times 150 \times 300 \ \mu m^3$ in size.

Raman spectroscopy setup. The Raman spectra presented here were obtained on a custom-built, low-temperature mi-

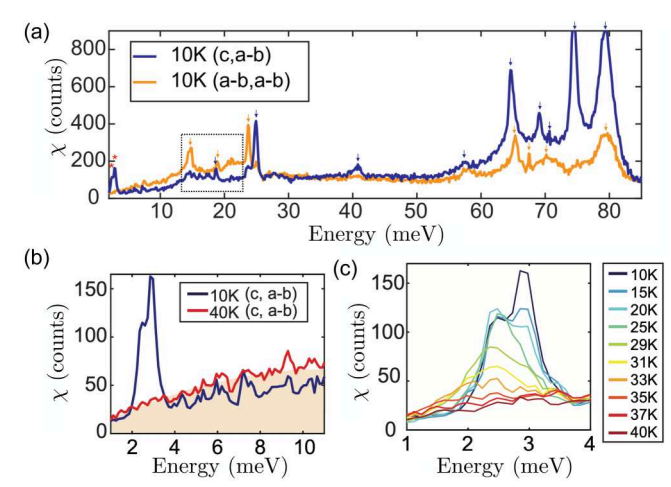


FIG. 2. (a) Raman susceptibility of β -LiIrO₃ at 10 K; the orange line shows (**a-b**, **a-b**) polarization, and the blue line is (**c**, **a-b**) polarization (orange and blue arrows indicate phonon modes in the $A_g + B_{1g}$ channels and the $B_{2g} + B_{3g}$ channels, respectively; red asterisks indicate two low-energy one-magnon peaks, and the dashed box encloses the multipeak structure between 12 and 22 meV). (b) Comparison of Raman susceptibility in the (**c**, **a-b**) channel at 10 K (blue) and 40 K (red). (c) Temperature dependence of the two low-energy peaks, M1 and M2, seen in the (**c**, **a-b**) channel.

croscopy setup [21,33,34]. A 532 nm excitation laser, whose spot has a diameter of 2 μ m, was used with the power limited to 10 μ W to minimize sample heating while allowing for a strong enough signal. The absence of laser-induced heating was crucial to ensure the ordered state is achieved and is confirmed via Stokes/anti-Stokes analysis as well as the appearance of magnons at the appropriate temperature. The single crystal was mounted with silver paint onto a copper sample holder and vacuum transferred onto the xyz stage in the cryostat [33]. At both room temperature and base temperature (10 K), the reported spectra were averaged from three spectra in the same environment to ensure reproducibility. The spectrometer had a 2400 g/mm grating, with an Andor CCD, providing a resolution of $\approx 1 \text{ cm}^{-1}$. Dark counts were removed by subtracting data collected with the same integration time with the laser blocked. To minimize the effects of hysteresis from the crystal structural transition, data were taken by first cooling the crystal to base temperature and then heating it to the target temperature.

Results. Figure 2(a) shows the 10 K Raman susceptibility measurement at cross (**c**, **a-b**) and parallel (**a-b**, **a-b**) polarizations. The notations (**c**, **a-b**) and (**a-b**, **a-b**) refer to the incident and scattered beam polarizations in the orthorhombic reference frame of the crystal structure. As the Raman intensity of Stokes and anti-Stokes scattering can be described using $I_{\text{Stokes}} = \chi(n_B + 1)$ and $I_{\text{anti-Stokes}} = \chi(n_B)$, we extracted the Raman susceptibility by dividing the measured intensity by the appropriate Bose function.

(i) Phonon modes. In both polarizations, the spectra show a number of sharp peaks superimposed on a continuum background. The very sharp peaks appearing above \sim 25 meV can be readily identified as optical phonon modes (obeying the selection rules of the *Fddd* space group), as was

analyzed previously in [15]. Among them, several peaks have pronounced asymmetric line shapes, which can be ascribed to Fano resonances [35] due to the coupling of the optical phonons to an underlying continuum of nonphononic origin. A similar asymmetry of the low-energy phonon line shapes has been extensively discussed in studies of bulk α -RuCl₃, both experimentally [14,18–20,36] and theoretically [37,38].

(ii) Sharp low-energy peaks. We now turn to low energies and low temperatures, where coherent magnons are most likely to appear. In Fig. 2(b), we plot the Raman spectra in the $(\mathbf{c}, \mathbf{a} \cdot \mathbf{b})$ polarization both at 10 K, the lowest temperature in our measurements, and at 40 K, slightly above T_I . We observe two nearby but well-resolved peaks at very low energy. Importantly, these peaks appear only in the cross polarization and are absent in the $(\mathbf{a} \cdot \mathbf{b}, \mathbf{a} \cdot \mathbf{b})$ data in Fig. 2(a). Moreover, at 10 K, the sharp modes and the underlying broad continuum coexist, while at 40 K only the broad continuum survives, suggesting that the former comes from magnons.

To better understand the low-energy sharp features, we focus on the (**c**, **a-b**) polarization and study their temperature evolution by performing the Raman scattering with a small step temperature increase [see data in Fig. 2(c)]. At 10 K, the two peaks are centered around 2.5 meV (M1) and 3 meV (M2), similar to the two sharp resonances centered around 2.1 and 3 meV that were previously observed in the terahertz spectra [39]. Interestingly, the intensity of the M2 peak is larger than the intensity of the M1 peak. However, the two peaks exhibit very different temperature evolutions. From 10 to 29 K, the intensity of the M2 peak decreases with temperature and is merged into the high-energy tail of M1, while that of M1 increases from 20 to 25 K and then starts decreasing and softening until it disappears as we reach T_I .

The fact that the two low-energy peaks exist only below T_I implies that they can be assigned to magnons. To establish this we employ the recently revised theory of Raman scattering mentioned above (see the Supplemental Material (SM), Secs. S2 and S3 [40]). As shown in Ref. [30], for the case of β -Li₂IrO₃ (and for $\Omega \ll \omega_{\rm in, out}$), the non-LF terms in Fig. 1(d) give rise to a sharp, one-magnon peak in the (a-c) channel. Figure 3 shows this peak for the present case of (c, **a-b**) polarization, as obtained from a semiclassical expansion around the commensurate $\mathbf{Q} = (2/3, 0, 0)$ approximant state of β -Li₂OIr₃ and using the minimal J-K- Γ model (see the SM, Sec. S1 [40]). At the level of linear spin-wave (LSW) theory (dashed black line), the position of the peak is centered around $\omega_2 \simeq 2.8$ meV, close to the positions of the observed peaks, M1 and M2. The same calculation for the (a-b, a-b) channel shows no peak in this energy range, consistent with the experimental results. This agreement on the position of the peak and its polarization dependence gives strong support to the one-magnon origin of one of the two peaks.

What about *the second peak*? To address this question we begin by recognizing that the noninteracting magnon spectrum does, in fact, feature a second low-energy mode at $\omega_1 \simeq 0.34$ meV (this is the mode that "unfolds" to the pseudo-Goldstone mode at the ordering wave vector in the dynamical structure factor; see [30]) but the calculated Raman intensity of this mode at $\mathbf{Q} = 0$ vanishes. Magnon anharmonicities (treated at the level of a mean-field decoupling of the quartic interactions and disregarding the magnon decay

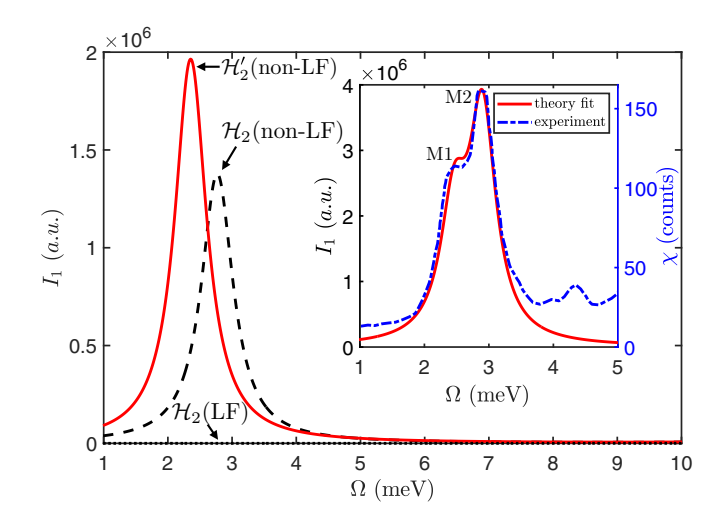


FIG. 3. The one-magnon Raman response computed within the non-LF theory at the level of linear spin wave theory (black dashed line) or with magnons renormalized by only the quartic interactions \mathcal{H}_4 (red solid line; see detailed discussion in Sec. S1 of the SM [40]) shows one low-energy sharp peak feature in the (\mathbf{c} , \mathbf{a} - \mathbf{b}) polarization channel. In contrast, the LSW theory with the LF Raman operator gives no low-energy features (black dotted line; not visible because the intensity vanishes). The inset shows the fit of low-energy peaks M1 and M2 to the phenomenological model discussed in Sec. S1 of the SM [40].

processes driven by the cubic terms; see the SM, Sec. S1 [40]) appear to be able to bring the two low-energy magnon modes much closer in energy (the renormalized energies are $\omega_1^{\rm ren} \simeq$ 2.3 meV and $\omega_2^{\rm ren} \simeq 3.1$ meV), as in experiment; however, we still see only one mode with nonzero intensity. This indicates that the vanishing of the intensity is due to a phase cancellation related to the commensurate character of the considered approximate ground state, in conjunction with the uniform character of the Raman vertex (similar to the vanishing of the intensity of the dynamical spin structure factor at the zone center in bipartite Néel antiferromagnets [41]). It is then plausible that incorporating the true IC character of the ordered state or lower-symmetry terms that are inevitably present in the spin Hamiltonian would remove this phase cancellation of the transition matrix element and render the second magnon mode observable as well. A simple phenomenological way to incorporate such a coupling by hand into our semiclassical expansion is discussed in Sec. S1 of the SM [40] and can readily deliver good agreement with experiment (see the inset in Fig. 3). Altogether, this suggests that the observed proximity of peaks M1 and M2 could well be a manifestation of strong anharmonicities, which is perhaps not surprising given the noncoplanar ordering and the strong anisotropic interactions in this material.

(iii) Multipeak structure at intermediate energies. Unlike the sharp low-energy modes M1 and M2, the origin of the multipeak structure observed at intermediate energies cannot be readily identified, especially in the region between 10 and 50 meV, where we expect a mixture of one- and two-magnon excitations along with overlapping phonon modes that are difficult to disentangle. Specifically, the reference calculations obtained at the LSW level in Ref. [30] have revealed

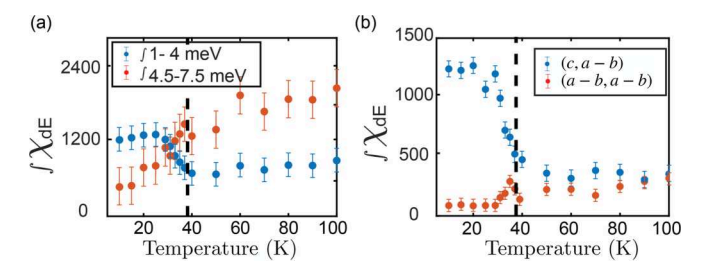


FIG. 4. (a) The SW in the (**c**, **a-b**) polarization: The red dots show the SW from 1 to 4 meV, which includes both the M1 and M2 modes; the blue dots represent the SW from 4.5 to 7.5 meV, which incorporates a 3 meV interval of the broad continuum with no magnon contribution. (b) The SW from 2 to 4 meV vs *T* for the (**a-b**, **a-b**) (red) and (**c**, **a-b**) (blue) polarizations.

a superposition of many one- and two-magnon modes due to the complex, multisublattice nature of the ordered state and the large number of resulting magnon branches [42,43]. Most notably, the results point to a polarization-dependent, multiple-peak structure from 12 to 22 meV, along with a broad (but still structured) two-magnon continuum between 15 and 45 meV. These features can qualitatively account for some of the structures seen in the experimental data. However, a more accurate description must take into account the effects of spin-wave anharmonicities and magnon decays, which are expected to play a nontrivial role in this intermediate-energy range, given the noncoplanar ordering and the strong off-diagonal Γ couplings, which are additional sources of the final-state interactions [44].

(iv) Magnetic continuum. Let us now return to the continuum background seen in the data. One of the most notable features of this continuum is that it covers a wide energy range, extending all the way down to zero energy, well below the onset of the two-magnon continuum expected for the IC ordered state [30]. Moreover, as mentioned above, unlike the sharp low-energy modes M1 and M2, which disappear at T_I , the broad continuum persists well above T_I [see Figs. 2(b) and 2(c)]. In fact, as we analyze further in Fig. 4, the broad continuum persists in a wide temperature range, extending up to ~ 100 K, well above T_I . The presence and very weak T dependence of the continuum as we cross T_I should be contrasted with what happens, e.g., in unfrustrated magnets, in which, with increasing T, the spectral weight broadens and shifts to lower energies and finally evolves to quasielastic scattering from overdamped short-range magnetic fluctuations above the ordering temperature [15,45–47]. This suggests that in β -Li₂IrO₃ much of the continuum background, especially its part persisting down to zero energy (where neither magnons nor phonons are expected, as mentioned above), is not related to magnons. On the other hand, such a continuum Raman response in which low-energy photons create pairs of Majorana spinons (no fluxes) with a bandwidth twice the Majorana spinon bandwidth is generally expected in the proximate Kitaev spin liquids [13–17,48–51].

To explore this further, we follow previous studies and proceed to analyze the integrated Raman susceptibility, or the spectral weight (SW). Figure 4(a) shows the T dependence of the SW in the (c, a-b) polarization in two energy ranges:

one between 1 and 4 meV, which includes both the M1 and M2 modes and the underlying continuum, and the other between 4.5 and 7.5 meV from only the continuum. We can see that the lower-energy SW, governed primarily by the two low-energy magnon modes, rapidly decreases with T until it reaches T_I , above which it shows nearly no T dependence. By contrast, the higher-energy SW, which comes solely from the continuum background, keeps increasing with T even above T_{I} , until it roughly levels off around 100 K. This points to a systematic SW transfer from magnons to the continuum background as we approach T_I . Conceptually, this ties in with the intuitive picture of magnons turning into pairs of deconfined spinons of the proximate Kitaev phase as we enter the paramagnetic phase. Next, we compare the low-energy SW obtained in the (c, a-b) and (a-b, a-b) polarizations [see Fig. 4(b)]. At low T, the (c, a-b) SW is significantly larger than the (a-b, a-b) SW due to the presence of the low-energy magnon modes in the former channel. Above T_I , the two SWs, both originating solely from the continuum background, saturate to some temperature-independent values, with the (c, a-b) SW being slightly larger than the (a-b, a-b) SW, consistent with the theoretical prediction for the pure Kitaev model on a hyperhoneycomb lattice [49].

Summary. Our inelastic Raman scattering data provide significant insights into the magnetic response of the hyperhoneycomb Kitaev magnet β -Li₂IrO₃ in a wide energy and temperature range. In our study, we have provided evidence that while the observed continuum background is likely of magnetic origin, it *cannot* be associated with the magnon excitations of the low-temperature ordered phase. The systematic transfer of spectral weight from the sharp low-energy peaks M1 and M2 (which we have established are magnons) to the continuum background as we heat up the system is consistent with the interpretation of the continuum in terms of fractional excitations emerging from the proximate spin liquid phase, as discussed in previous studies [13–15,17,22,50].

Turning to the sharp low-energy peaks M1 and M2, we have demonstrated numerically that their temperature and polarization dependence can be explained only by extending the traditional Loudon-Fleury theory of Raman scattering, in which the contribution \mathcal{R}_{ij} to the Raman vertex from a given bond \mathbf{d}_{ij} is given by the corresponding superexchange Hamiltonian \mathcal{H}_{ij} weighted by a bond-specific polarizationdependent factor. In reality, \mathcal{R}_{ij} can have a different functional form than \mathcal{H}_{ii} , as the various electron hopping paths each come with their own nonequivalent polarization factors [30]. In the present case, we have shown that the observed peaks M1 and M2 verify the existence of the non-Loudon-Fleury dipole terms that arise from the interplay of direct and ligandmediated hopping, similar to the exchange terms leading to the Γ interaction. This experimental verification therefore marks a drastic change in paradigm for the understanding of Raman scattering in materials with strong SOC and multiple exchange paths.

Acknowledgments. We thank M. Li for earlier collaborations on related topics. Y.Y. and N.B.P. acknowledge the support from the U.S. Department of Energy, Office of Science, Basic Energy Sciences. under Award No. DE-SC0018056. The work done by Y.W. was supported by the

Office of Naval Research under Award No. N00014-20-1-2308. K.S.B. is grateful for the support of the U.S. Department of Energy, Office of Science, Office of Basic Energy Sciences, under Award No. DE-SC0018675. The work of I.R. was supported by the Engineering and Physical Sciences Research Council [Grant No. EP/V038281/1]. Work by J.G.A.

and A.R. was supported by the Department of Energy Early Career Program, Office of Basic Energy Sciences, Materials Sciences and Engineering Division, under Contract No. DE-AC02-05CH11231 for crystal growth. A.R. also acknowledges support from the University of California President Postdoctoral Fellowship Program.

- [1] A. Kitaev, Ann. Phys. (NY) 321, 2 (2006).
- [2] G. Jackeli and G. Khaliullin, Phys. Rev. Lett. 102, 017205 (2009).
- [3] J. Chaloupka, G. Jackeli, and G. Khaliullin, Phys. Rev. Lett. 105, 027204 (2010).
- [4] Frontiers of 4d- and 5d-Transition Metal Oxides, edited by G. Cao and L. DeLong (World Scientific, Singapore, 2013).
- [5] W. Witczak-Krempa, G. Chen, Y. B. Kim, and L. Balents, Annu. Rev. Condens. Matter Phys. 5, 57 (2014).
- [6] J. G. Rau, E. K.-H. Lee, and H.-Y. Kee, Annu. Rev. Condens. Matter Phys. 7, 195 (2016).
- [7] S. M. Winter, A. A. Tsirlin, M. Daghofer, J. van den Brink, Y. Singh, P. Gegenwart, and R. Valenti, J. Phys.: Condens. Matter 29, 493002 (2017).
- [8] H. Takagi, T. Takayama, G. Jackeli, G. Khaliullin, and S. E. Nagler, Nat. Rev. Phys. 1, 264 (2019).
- [9] S. Trebst and C. Hickey, Phys. Rep. 950, 1 (2022).
- [10] R. Schaffer, S. Bhattacharjee, and Y. B. Kim, Phys. Rev. B 86, 224417 (2012).
- [11] J. G. Rau, E. K.-H. Lee, and H.-Y. Kee, Phys. Rev. Lett. 112, 077204 (2014).
- [12] I. Rousochatzakis, J. Reuther, R. Thomale, S. Rachel, and N. B. Perkins, Phys. Rev. X 5, 041035 (2015).
- [13] A. Banerjee, J. Yan, J. Knolle, C. A. Bridges, M. B. Stone, M. D. Lumsden, D. G. Mandrus, D. A. Tennant, R. Moessner, and S. E. Nagler, Science 356, 1055 (2016).
- [14] L. J. Sandilands, Y. Tian, K. W. Plumb, Y.-J. Kim, and K. S. Burch, Phys. Rev. Lett. 114, 147201 (2015).
- [15] A. Glamazda, P. Lemmens, S. H. Do, Y. S. Choi, and K. Y. Choi, Nat. Commun. 7, 12286 (2016).
- [16] J. Nasu, J. Knolle, D. L. Kovrizhin, Y. Motome, and R. Moessner, Nat. Phys. 12, 912 (2016).
- [17] I. Rousochatzakis, S. Kourtis, J. Knolle, R. Moessner, and N. B. Perkins, Phys. Rev. B **100**, 045117 (2019).
- [18] D. Wulferding, Y. Choi, S.-H. Do, C. H. Lee, P. Lemmens, C. Faugeras, Y. Gallais, and K.-Y. Choi, Nat. Commun. 11, 1603 (2020).
- [19] A. Sahasrabudhe, D. A. S. Kaib, S. Reschke, R. German, T. C. Koethe, J. Buhot, D. Kamenskyi, C. Hickey, P. Becker, V. Tsurkan, A. Loidl, S. H. Do, K. Y. Choi, M. Grüninger, S. M. Winter, Z. Wang, R. Valentí, and P. H. M. van Loosdrecht, Phys. Rev. B 101, 140410(R) (2020).
- [20] D. Lin, K. Ran, H. Zheng, J. Xu, L. Gao, J. Wen, S.-L. Yu, J.-X. Li, and X. Xi, Phys. Rev. B **101**, 045419 (2020).
- [21] Y. Wang, G. B. Osterhoudt, Y. Tian, P. Lampen-Kelley, A. Banerjee, T. Goldstein, J. Yan, J. Knolle, H. Ji, R. J. Cava, J. Nasu, Y. Motome, S. E. Nagler, D. Mandrus, and K. S. Burch, npj Quantum Mater. 5, 14 (2020).
- [22] A. Ruiz, N. P. Breznay, M. Li, I. Rousochatzakis, A. Allen, I. Zinda, V. Nagarajan, G. Lopez, Z. Islam, M. H. Upton, J. Kim,

- A. H. Said, X.-R. Huang, T. Gog, D. Casa, R. J. Birgeneau, J. D. Koralek, J. G. Analytis, N. B. Perkins, and A. Frano, Phys. Rev. B 103, 184404 (2021).
- [23] A. Biffin, R. D. Johnson, S. Choi, F. Freund, S. Manni, A. Bombardi, P. Manuel, P. Gegenwart, and R. Coldea, Phys. Rev. B 90, 205116 (2014).
- [24] T. Takayama, A. Kato, R. Dinnebier, J. Nuss, H. Kono, L. S. I. Veiga, G. Fabbris, D. Haskel, and H. Takagi, Phys. Rev. Lett. 114, 077202 (2015).
- [25] A. Ruiz, A. Frano, N. P. Breznay, I. Kimchi, T. Helm, I. Oswald, J. Y. Chan, R. J. Birgeneau, Z. Islam, and J. G. Analytis, Nat. Commun. 8, 961 (2017).
- [26] A. Ruiz, V. Nagarajan, M. Vranas, G. Lopez, G. T. McCandless, I. Kimchi, J. Y. Chan, N. P. Breznay, A. Frañó, B. A. Frandsen, and J. G. Analytis, Phys. Rev. B 101, 075112 (2020).
- [27] M. Majumder, F. Freund, T. Dey, M. Prinz-Zwick, N. Büttgen, Y. Skourski, A. Jesche, A. A. Tsirlin, and P. Gegenwart, Phys. Rev. Materials 3, 074408 (2019).
- [28] V. M. Katukuri, S. Nishimoto, V. Yushankhai, A. Stoyanova, H. Kandpal, S. Choi, R. Coldea, I. Rousochatzakis, L. Hozoi, and J. van den Brink, New J. Phys. 16, 013056 (2014).
- [29] I. Rousochatzakis and N. B. Perkins, Phys. Rev. Lett. 118, 147204 (2017).
- [30] Y. Yang, M. Li, I. Rousochatzakis, and N. B. Perkins, Phys. Rev. B 104, 144412 (2021).
- [31] P. A. Fleury and R. Loudon, Phys. Rev. 166, 514 (1968).
- [32] B. S. Shastry and B. I. Shraiman, Phys. Rev. Lett. 65, 1068 (1990).
- [33] Y. Tian, A. A. Reijnders, G. B. Osterhoudt, I. Valmianski, J. G. Ramirez, C. Urban, R. Zhong, J. Schneeloch, G. Gu, I. Henslee, and K. S. Burch, Rev. Sci. Instrum. 87, 043105 (2016).
- [34] G. B. Osterhoudt, Y. Wang, C. A. C. Garcia, V. M. Plisson, J. Gooth, C. Felser, P. Narang, and K. S. Burch, Phys. Rev. X 11, 011017 (2021).
- [35] U. Fano, Phys. Rev. **124**, 1866 (1961).
- [36] T. T. Mai, A. McCreary, P. Lampen-Kelley, N. Butch, J. R. Simpson, J.-Q. Yan, S. E. Nagler, D. Mandrus, A. R. Hight Walker, and R. V. Aguilar, Phys. Rev. B 100, 134419 (2019).
- [37] A. Metavitsiadis, W. Natori, J. Knolle, and W. Brenig, Phys. Rev. B 105, 165151 (2022).
- [38] K. Feng, S. Swarup, and N. B. Perkins, Phys. Rev. B 105, L121108 (2022).
- [39] M. Majumder, M. Prinz-Zwick, S. Reschke, A. Zubtsovskii, T. Dey, F. Freund, N. Büttgen, A. Jesche, I. Kézsmárki, A. A. Tsirlin, and P. Gegenwart, Phys. Rev. B 101, 214417 (2020).
- [40] See Supplemental Material at http://link.aps.org/supplemental/ 10.1103/PhysRevB.105.L241101 for technical details of spinwave theory for the minimal Hamiltonian describing the properties of β-Li₂IrO₃ (Sec. S1), the non-Loudon-Fleury formalism of magnetic Raman scattering (Sec. S2), and

- one-magnon Raman response in β -Li₂IrO₃ (Sec. S3). In Sec. S4 we provide additional plots to show the evolution of the Raman spectra for a wide range of energies and temperatures.
- [41] N. S. Headings, S. M. Hayden, R. Coldea, and T. G. Perring, Phys. Rev. Lett. 105, 247001 (2010).
- [42] S. Ducatman, I. Rousochatzakis, and N. B. Perkins, Phys. Rev. B 97, 125125 (2018).
- [43] M. Li, I. Rousochatzakis, and N. B. Perkins, Phys. Rev. Research 2, 013065 (2020).
- [44] S. M. Winter, K. Riedl, P. A. Maksimov, A. L. Chernyshev, A. Honecker, and R. Valenti, Nat. Commun. 8, 1152 (2017).
- [45] T. Martin, R. Merlin, D. Huffman, and M. Cardona, Solid State Commun. 22, 565 (1977).

- [46] R. Liu, M. Klein, D. Salamon, S. Cooper, W. Lee, S.-W. Cheong, and D. Ginsberg, J. Phys. Chem. Solids 54, 1347 (1993).
- [47] H. Gretarsson, N. H. Sung, M. Höppner, B. J. Kim, B. Keimer, and M. Le Tacon, Phys. Rev. Lett. 116, 136401 (2016).
- [48] J. Knolle, G.-W. Chern, D. L. Kovrizhin, R. Moessner, and N. B. Perkins, Phys. Rev. Lett. **113**, 187201 (2014).
- [49] B. Perreault, J. Knolle, N. B. Perkins, and F. J. Burnell, Phys. Rev. B 92, 094439 (2015).
- [50] Y. Yamaji, T. Suzuki, and M. Kawamura, arXiv:1802.02854.
- [51] G. B. Halász, S. Kourtis, J. Knolle, and N. B. Perkins, Phys. Rev. B 99, 184417 (2019).